Split Bregman Method for Minimization of Region-Scalable Fitting Energy for Image Segmentation

Yunyun Yang[a,b], Chunming Li[c], Chiu-Yen Kao[a,d⋆], and Stanley Osher [e]

[a] Department of Mathematics, The Ohio State University, OH 43202, U.S.
[b] Department of Mathematics, Harbin Institute of Technology, Harbin, 150001, China
[c] Department of Radiology, University of Pennsylvania, PA 19104, U.S.
[d] Mathematical Biosciences Institute, The Ohio State University, OH 43210, U.S.
[e] Department of Mathematics, University of California, Los Angeles, CA 90095, U.S.

Abstract. In this paper, we incorporated the global convex segmentation method and the split Bregman technique into the region-scalable fitting energy model. The new proposed method based on the region-scalable model can draw upon intensity information in local regions at a controllable scale, so that it can segment images with intensity inhomogeneity. Furthermore, with the application of the global convex segmentation method and the split Bregman technique, the method is very robust and efficient. By using a non-negative edge detector function to the proposed method, the algorithm can detect the boundaries more easily and achieve results that are very similar to those obtained through the classical geodesic active contour model. Experimental results for synthetic and real images have shown the robustness and efficiency of our method and also demonstrated the desirable advantages of the proposed method.

Key words: split Bregman, region-scalable model, image segmentation, intensity inhomogeneity

1 Introduction

Image segmentation [1–4] is a fundamental and important task in image analysis and computer vision. Most of existing methods for image segmentation can be categorized into two classes: region-based methods [1, 5–9] and edge-based methods [3, 4, 10–13]. In general, the region-based methods are more robust than the edge-based methods. However, the former type of methods [1, 5–7] typically relies on the homogeneity of the image intensities, which is often not satisfied by real world images.

Intensity inhomogeneity has been a challenging difficulty for region-based methods. It often occurs in real images from different modalities such as medical

⋆ Corresponding author: Tel: 614-292-8609, Fax: 614-292-1479, kao@math.ohio-state.edu. This work is partially supported by DMS 0811003 and Sloan Fellowship.

images. Segmentation of such medical images usually requires intensity inhomogeneity correction as a preprocessing step [14]. Intensity inhomogeneity can be addressed by more sophisticated models than piecewise constant (PC) models. Two piecewise smooth (PS) models were proposed in Vese and Chan [9] and Tsai et al. [8] independently, aiming at minimizing the Mumford-Shah functional [15]. These PS models have exhibited certain capability of handling intensity inhomogeneity. However, they are computationally expensive and suffer from other difficulties. Michailovich et al. [16] proposed an active contour model which does not rely on the intensity homogeneity and, therefore, to some extent, overcomes the limitation of PC models. Recently, Li et al. [17] proposed an efficient region-based model, called a region-scalable fitting (RSF) energy model, which is able to deal with intensity inhomogeneities. The RSF model was formulated in a level set framework, which is quite sensitive to contour initialization.

Recently the split Bregman method has been adopted to solve image segmentation more efficiently. This method has the advantage that it does not require regularization, continuation or the enforcement of inequality constraints and therefore is extremely efficient. Several applications of the split Bregman method are Rudin-Osher-Fatemi (ROF) denoising [18–20] and image segmentation [21, 22]. In [19], they applied this technique to the ROF functional for image denoising and to a compressed sensing problem that arose in Magnetic Resonance Imaging. In [22], the authors applied the split Bregman concept to image segmentation problems and built fast solvers. However, this method was based on the PC model and thus it was not able to deal with intensity inhomogeneity.

In this paper, we incorporate the global convex segmentation (GCS) method and the split Bregman technique into the RSF model [17]. We first drop the regularization term of the original gradient flow equation in [17]. Following the idea in Chan et al. [23], we then get a simplified flow equation which has coincident stationary solution with the original one. In order to guarantee the global minimum, we restrict the solution to lie in a finite interval. Then we modify the simplified energy to incorporate information from the edge by using a non-negative edge detector function, and get results that are very similar to those obtained through the classical geodesic active contour (GAC) model [10]. We thus apply the split Bregman method to the proposed minimization problem of region-scalable fitting energy for segmentation and demonstrate many numerical results. As a result, the proposed algorithm can be used to segment images with intensity inhomogeneity efficiently.

The remainder of this paper is organized as follows. We first review some well-known existing region-based models and their limitations in Section 2. The new proposed method is introduced in Section 3. The implementation and results of our method are given in Section 4. This paper is concluded in Section 5.

2 Region-based Active Contour Models

2.1 Chan-Vese Model

Chan and Vese [1] proposed an active contour approach to the Mumford-Shah problem [15]. This image segmentation method works when the image consists of homogeneous regions. Let $\Omega \subset \Re^2$ be the image domain, and $I : \Omega \to \Re$ be a given gray level image, the idea is to find a contour C which segments the given image into non-overlapping regions. The model they proposed is to minimize the following energy:

$$\mathcal{F}^{CV}(C, c_1, c_2) = \lambda_1 \int_{outside(C)} |I(x) - c_1|^2 dx + \lambda_2 \int_{inside(C)} |I(x) - c_2|^2 dx + \nu |C| \,, \tag{1}$$

where λ_1, λ_2 and ν are positive constants, $outside(C)$ and $inside(C)$ represent the regions outside and inside the contour C, respectively, c_1 and c_2 are two constants that approximate the image intensities in $outside(C)$ and $inside(C)$, and $|C|$ is the length of the contour C. The optimal constants c_1 and c_2 that minimize the above energy turn out to be the averages of the intensities in the entire regions $outside(C)$ and $inside(C)$, respectively. For inhomogeneous images, as demonstrated in [17, 24], the PC model [1, 5, 9] may fail to provide correct image segmentation. Thus PS model [8, 9] was proposed to overcome this limitation. Instead of constant approximations c_1 and c_2 in PC model, two smooth functions u^+ and u^- were used to estimate the intensities outside and inside the contour C. However, this approach requires solving two elliptic PDEs for u^+ and u^- and one evolution equation for ϕ. The complexity of the algorithm limits its applications in practice.

2.2 Region-Scalable Fitting Energy Model

Recently, Li et al. [17] proposed a new region-based model to use the local intensity information in a scalable way. The energy functional they tried to minimize is:

$$\mathcal{E}(C, f_1(x), f_2(x)) = \sum_{i=1}^{2} \lambda_i \int [\int_{\Omega_i} K_\sigma(x - y) |I(y) - f_i(x)|^2 dy] dx + \nu |C| \,, \tag{2}$$

where $\Omega_1 = outside(C)$ and $\Omega_2 = inside(C)$, λ_1, λ_2 and ν are positive constants, and $f_1(x)$ and $f_2(x)$ are two functions that approximate image intensities in Ω_1 and Ω_2, respectively. The aim of the kernel function K_σ is to put heavier weights on points y which are close to the center point x. For simplicity, a Gaussian kernel with a scale parameter $\sigma > 0$ was used:

$$K_\sigma(u) = \frac{1}{2\pi\sigma^2} e^{-|u|^2/2\sigma^2} \,. \tag{3}$$

To handle topological changes, the authors in [17] converted (2) to a level set formulation.

As in level set methods [25], the contour $C \subset \Omega$ is represented by the zero level set of a level set function $\phi : \Omega \to \Re$. Thus, the energy $\mathcal{E}$ in (2) can be written as:

$$\mathcal{E}_\epsilon(\phi, f_1, f_2) = \int \mathcal{E}_\epsilon^x(\phi, f_1(x), f_2(x))dx + \nu \int |\nabla H_\epsilon(\phi(x))|dx \ , \tag{4}$$

where

$$\mathcal{E}_\epsilon^x(\phi, f_1(x), f_2(x)) = \sum_{i=1}^{2} \lambda_i \int K_\sigma(x-y)|I(y) - f_i(x)|^2 M_i^\epsilon(\phi(y))dy \tag{5}$$

is the region-scalable fitting energy, $M_1^\epsilon(\phi) = H_\epsilon(\phi)$ and $M_2^\epsilon(\phi) = 1 - H_\epsilon(\phi)$. H_ϵ is a smooth function approximating the Heaviside function H which is defined by:

$$H_\epsilon(x) = \frac{1}{2}[1 + \frac{2}{\pi}\arctan(\frac{x}{\epsilon})] \ . \tag{6}$$

In order to preserve the regularity of the level set function ϕ, they used a level set regularization term [12]:

$$\mathcal{P}(\phi) = \int \frac{1}{2}(|\nabla\phi(x)| - 1)^2 dx \ . \tag{7}$$

Therefore, the energy functional they proposed to minimize is:

$$\mathcal{F}(\phi, f_1, f_2) = \mathcal{E}_\epsilon(\phi, f_1, f_2) + \mu\mathcal{P}(\phi) \ , \tag{8}$$

where μ is a positive constant.

To minimize this energy functional, the standard gradient descent method is used. By calculus of variations, for a fixed level set function ϕ, the optimal functions $f_1(x)$, $f_2(x)$ that minimize $\mathcal{F}(\phi, f_1, f_2)$ are obtained by:

$$f_i(x) = \frac{K_\sigma(x) * [M_i^\epsilon(\phi(x))I(x))]}{K_\sigma(x) * M_i^\epsilon(\phi(x))}, \ i = 1, 2 \ . \tag{9}$$

For fixed f_1 and f_2, the level set function ϕ that minimizes $\mathcal{F}(\phi, f_1, f_2)$ can be obtained by solving the following gradient flow equation:

$$\frac{\partial\phi}{\partial t} = -\delta_\epsilon(\phi)(\lambda_1 e_1 - \lambda_2 e_2) + \nu\delta_\epsilon(\phi)div(\frac{\nabla\phi}{|\nabla\phi|}) + \mu[\nabla^2\phi - div(\frac{\nabla\phi}{|\nabla\phi|})] \ , \tag{10}$$

where δ_ϵ is the derivative of H_ϵ , and e_i $(i = 1 \ or \ 2)$ is defined as:

$$e_i(x) = \int K_\sigma(y-x)|I(x) - f_i(y)|^2 dy, \ i = 1, 2 \ . \tag{11}$$

3 Split Bregman Method for Minimization of Region-Scalable Fitting Energy

In this section we introduce a new region-scalable model which incorporates the GCS method and the split Bregman technique. In fact, the energy functional (4) of the RSF model in section 2.2 is nonconvex, so the evolution can be easily trapped to a local minimum. We thus apply the GCS method to the RSF model to make the fitting energy convex. The split Bregman technique is used to minimize the energy functional in a more efficient way. The proposed new model thus can improve the robustness and efficiency, while inheriting the desirable ability to deal with intensity inhomogeneity in image segmentation.

Considering the gradient flow equation (10), we first drop the last term which regularized the level set function to be close to a distance function:

$$\frac{\partial \phi}{\partial t} = \delta_\epsilon(\phi)[(-\lambda_1 e_1 + \lambda_2 e_2) - \nu div(\frac{\nabla \phi}{|\nabla \phi|})] \,, \tag{12}$$

without loss of generality, we take $\nu = 1$. The Chan-Vese Model can be considered as a special case of (12), i.e. $K_\sigma(y - x) = 1_\Omega/|\Omega|$.

Following the idea in Chan et al. [23], the stationary solution of (12) coincides with the stationary solution of:

$$\frac{\partial \phi}{\partial t} = [(-\lambda_1 e_1 + \lambda_2 e_2) - div(\frac{\nabla \phi}{|\nabla \phi|})] \,. \tag{13}$$

The simplified flow represents the gradient descent for minimizing the energy:

$$E(\phi) = |\nabla \phi|_1 + \langle \phi, \lambda_1 e_1 - \lambda_2 e_2 \rangle \,. \tag{14}$$

This energy does not have a unique global minimizer because it is homogeneous of degree one. By restricting the solution to lie in a finite interval, e.g. $a_0 \le \phi \le b_0$, the global minimum can be guaranteed, i.e.

$$\min_{a_0 \le \phi \le b_0} E(\phi) = \min_{a_0 \le \phi \le b_0} |\nabla \phi|_1 + \langle \phi, r \rangle \,, \tag{15}$$

where $r = \lambda_1 e_1 - \lambda_2 e_2$. Once the optimal ϕ is found, the segmented region can be found by thresholding the level set function for some $\alpha \in (a_0, b_0)$:

$$\Omega_1 = \{x : \phi(x) > \alpha\} \,. \tag{16}$$

As in [26], we modify the energy (15) to incorporate information from an edge detector. This is accomplished by using the weighted TV norm:

$$TV_g(\phi) = \int g|\nabla \phi| = |\nabla \phi|_g \,, \tag{17}$$

where g is the non-negative edge detector function. One common choice for the edge detector is:

$$g(\xi) = \frac{1}{1 + \beta|\xi|^2} \,, \tag{18}$$

where β is a parameter that determines the detail level of the segmentation. By replacing the standard TV norm $TV(\phi) = \int |\nabla\phi| = |\nabla\phi|_1$ in (15) with the weighted version (17), we make the model more likely to favor segmentation along curves where the edge detector function is minimal. Then the minimization problem becomes:

$$\min_{a_0\le\phi\le b_0} E(\phi) = \min_{a_0\le\phi\le b_0} |\nabla\phi|_g + \langle\phi, r\rangle \ . \tag{19}$$

To apply the split Bregman approach [22] to (19), we introduce the auxillary variable, $\overrightarrow{d} \leftarrow \nabla\phi$. To weakly enforce the resulting equality constraint, we add a quadratic penalty function which results in the following unconstrained problem:

$$(\phi^*, \overrightarrow{d}^*) = arg \min_{a_0\le\phi\le b_0} |\overrightarrow{d}|_g + \langle\phi, r\rangle + \frac{\lambda}{2} \parallel \overrightarrow{d} - \nabla\phi \parallel^2 \ . \tag{20}$$

We then apply Bregman iteration to strictly enforce the constraint $\overrightarrow{d} = \nabla\phi$. The resulting optimization problem is:

$$(\phi^{k+1}, \overrightarrow{d}^{k+1}) = arg \min_{a_0\le\phi\le b_0} |\overrightarrow{d}|_g + \langle\phi, r\rangle + \frac{\lambda}{2} \parallel \overrightarrow{d} - \nabla\phi - \overrightarrow{b}^k \parallel^2 \ . \tag{21}$$

$$\overrightarrow{b}^{k+1} = \overrightarrow{b}^k + \nabla\phi^{k+1} - \overrightarrow{d}^{k+1} \ . \tag{22}$$

For fixed $\overrightarrow{d}$, the Euler-Lagrange equation of optimization problem (21) with respect to ϕ is:

$$\triangle\phi = \frac{r}{\lambda} + \nabla\cdot(\overrightarrow{d} - \overrightarrow{b}), \text{ whenever } a_0 < \phi < b_0 \ . \tag{23}$$

By using central discretization for Laplace operator and backward difference for divergence operator, the numerical scheme for (23) is:

$$\alpha_{i,j} = d^x_{i-1,j} - d^x_{i,j} + d^y_{i,j-1} - d^y_{i,j} - (b^x_{i-1,j} - b^x_{i,j} + b^y_{i,j-1} - b^y_{i,j}) \ . \tag{24}$$

$$\beta_{i,j} = \frac{1}{4}(\phi_{i-1,j} + \phi_{i+1,j}\phi_{i,j-1} + \phi_{i,j+1} - \frac{r}{\lambda} + \alpha_{i,j}) \ . \tag{25}$$

$$\phi_{i,j} = \max\{\min\{\beta_{i,j}, b_0\}, a_0\} \ . \tag{26}$$

For fixed ϕ, minimization of (21) with respect to $\overrightarrow{d}$ gives:

$$\overrightarrow{d}^{k+1} = shrink_g(\overrightarrow{b}^k + \nabla\phi^{k+1}, \frac{1}{\lambda}) = shrink(\overrightarrow{b}^k + \nabla\phi^{k+1}, \frac{g}{\lambda}) \ , \tag{27}$$

where

$$shrink(x, \gamma) = \frac{x}{|x|}\max(|x| - \gamma, 0) \ . \tag{28}$$

4 Implementation and Experimental Results

4.1 Implementation

The split Bregman algorithm for the minimization problem (19) in section 3 can be summarized as follows:

1: while $\| \phi^{k+1} - \phi^k \| > \epsilon$ do
2: Define $r^k = \lambda_1 e_1^k - \lambda_2 e_2^k$
3: $\phi^{k+1} = GS(r^k, \overrightarrow{d}^k, \overrightarrow{b}^k, \lambda)$
4: $\overrightarrow{d}^{k+1} = shrink_g(\overrightarrow{b}^k + \nabla\phi^{k+1}, \frac{1}{\lambda})$
5: $\overrightarrow{b}^{k+1} = \overrightarrow{b}^k + \nabla\phi^{k+1} - \overrightarrow{d}^{k+1}$
6: Find $\Omega_1^k = \{x : \phi^k(x) > \alpha\}$
7: Update e_1^k and e_2^k
8: end while

Here, we have used $GS(r^k, \overrightarrow{d}^k, \overrightarrow{b}^k, \lambda)$ to denote one sweep of the Gauss-Seidel formula (24)-(26).

In this paper, the level set function ϕ can be simply initialized as a binary step function which takes a constant value b_0 inside a region and another constant value a_0 outside. Then the thresholding value α is chosen as $\alpha = (a_0 + b_0)/2$ when one needs to find the segmented region $\Omega_1 = \{x : \phi(x) > \alpha\}$. We choose $a_0 = 0$, $b_0 = 1$ in most of the experiments shown in this paper, while for some images, we will choose different values to get better result or faster convergence. The details will be shown in next subsection 4.2. In our implementation, the functions f_1 and f_2 are updated at every time step according to (9) before the update of the level set function ϕ. As in [17], in order to compute the convolutions in (9) more efficiently, the kernel K_σ can be truncated as a $w \times w$ mask, here we also choose $w = 4\sigma + 1$. For most of our experiments, the scale parameter is chosen as $\sigma = 3.0$ unless specified.

4.2 Results

The proposed method has been tested with synthetic and real images from different modalities. Unless otherwise specified, we use the following parameters in this paper: $\sigma = 3.0$, $a_0 = 0$, $b_0 = 1$, $\epsilon = 1$, and $\lambda = 0.001$. We use $\beta = 100$ for all images except for the brain image in the last column of Fig. 2 we use $\beta = 10$, and for the noisy synthetic images in column 1 of Fig. 2 and row 3 of Fig. 3 we choose $\beta = 20$. We use $\lambda_1 = 1.1e-5$, $\lambda_2 = 1e-5$ for most images in this paper, for several other images we use different parameters λ_1, λ_2 for better and faster results. In general, our method with a small scale σ can produce more accurate location of the object boundaries.

We first show the result for a synthetic inhomogeneous image in Fig. 1. Column 1 is the original image with the initial contour, column 2 is the result of our method, column 3 is the result of the split Bregman on PC model in [22]. From this figure, we can see the advantage of our proposed method for inhomogeneous

image. Our method can segment the images correctly even though the image is very inhomogeneous, while the split Bregman on PC model cannot segment it correctly as shown in column 3.

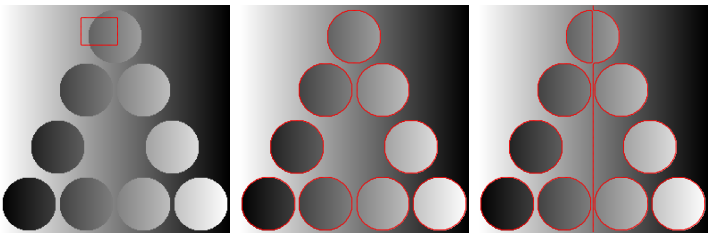

Fig. 1. Segmentation of a synthetic image with our proposed method and split Bregman on PC model. Column 1: the original image and the initial contour. Column 2: the result of our proposed method. Column 3: the result of the split Bregman on PC model

Fig. 2 shows the results for one synthetic image, one X-ray image of vessel, and two real images of a T-shaped object and an MR image from left to right. All of them are typical images with intensity inhomogeneity. The top row are the original images with the initial contours, the bottom row are the results with the final contours. As shown in Fig. 2, our method successfully extracts the object boundaries for these challenging images. For the images in the first two columns, we choose $\lambda_1 = \lambda_2 = 1e-5$. For the real brain image in the last column, we use $\lambda_1 = 1.25e-5$ and $\lambda_2 = 1e-5$ in order to put a larger penalty on the area of $inside(C)$. In this way the emergence of new contour outside the initial contour, which would increase the area of $inside(C)$, is to some extent prevented.

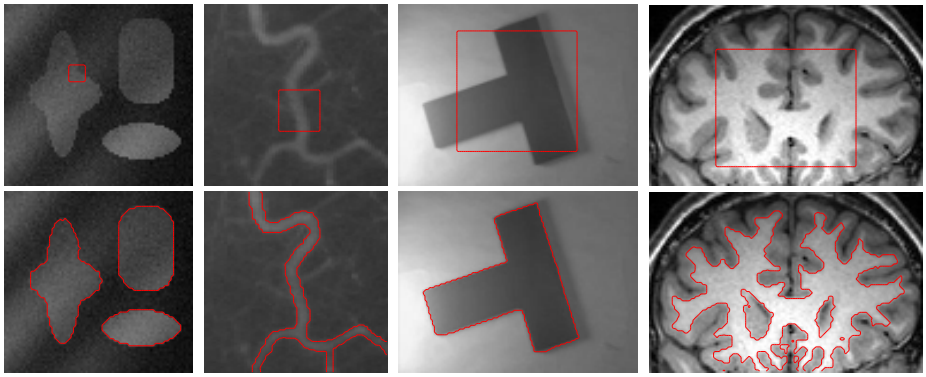

Fig. 2. Results of our method for synthetic images and real images. Top row: original images with initial contours. Bottom row: segmentation results with final contours

The results in Fig. 2 are similar to the results with the original RSF model in [17]. However, by comparing the computational procedures in the original RSF model and our model, it is clear that our method is more efficient than the RSF model because we apply the split Bregman approach to the optimization problem. This is demonstrated by comparing the iteration number and computation time in both methods for four images in Table 1, which were recorded from our experiments with Matlab code run on a Dell Precision 390 PC, Genuine Intel(R) Xeon (R), X7350, 2.93 GHz, 4 GB RAM, with Matlab 7.9. The sizes of these images are also shown in this table. In the experiments with the images in Fig. 2, the CPU time of our model is about one second.

Table 1. Iteration number and CPU time (in second) for our model and RSF model for the images in Fig. 2 in the same order. The sizes of images are 75×79, 110×110, 96×127, and 78×119 pixels, respectively

	image1	image2	image3	image4
Our model	32(0.33)	67(1.13)	26(0.49)	48(0.70)
RSF model	200(1.40)	150(1.74)	300(3.72)	300(3.01)

We show the results for three synthetic flower images in Fig. 3. These images all have the same flower in the center but different distribution of intensities. The curve evolution process from the initial contour to the final contour is shown in every row for the corresponding image. The intensity of the image in the first row is piecewise constant. The second and third rows in Fig. 3 show the results for two images corrupted by intensity inhomogeneity. The image in third row was generated by adding random noise to the clean image in the second row. The standard deviation of the noise is 5.0. We can see that the segmentation results for the clean image and the noise contaminated version are very close. This demonstrates the robustness of our method to the noise.

Then we show the result for another synthetic image in Fig. 4. This image has been used in [1], there are three objects in this image with different intensities. The initial and the final contours are plotted on the images in the first row and the second row, respectively. The first column is the result for the piecewise constant image, the second column shows the result for the image corrupted by intensity inhomogeneity in the background. In this experiment, we choose $a_0 = -2,\ b_0 = 2$ instead of $a_0 = 0,\ b_0 = 1,$ because when $a_0 = 0,\ b_0 = 1$ are chosen, the algorithm fails to detect the interior contour correctly as shown in the third and the fourth columns. We choose $\lambda_1 = \lambda_2 = 2e - 6$ for the inhomogeneous images in the second and the fourth columns. From the second column, we can see that the intensity in the background is inhomogeneous and part of the background has very close intensities to the circular ring, but our method can successfully extract the object boundary in this image. The results

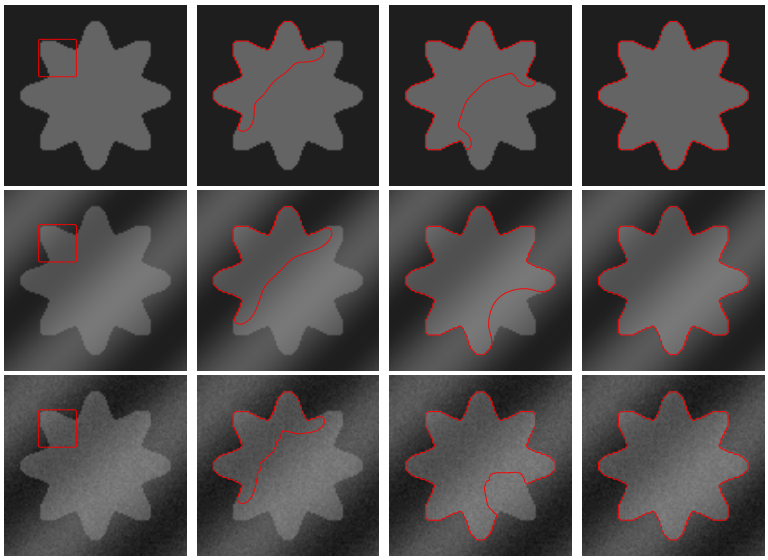

Fig. 3. Results of our method for three synthetic images. The curve evolution process from the initial contour (in the first column) to the final contour (in the fourth column) is shown in every row for the corresponding image

also show that our method is able to segment images with multiple distinct means of image intensities.

In Fig. 5, we apply our model to a color image of flower. In this experiment, we choose $a_0 = -2$, $b_0 = 2$ and $\lambda_1 = \lambda_2 = 2e - 6$. The evolution of active contours from its initial state to the converged state is shown. This experiment shows that our method can also segment color images well.

5 Conclusion

This paper incorporated the GCS method and the split Bregman technique into the RSF model, which was originally formulated in a level set framework for segmentation of inhomogeneous images. The proposed method significantly improves the efficiency and robustness of the RSF model, while inheriting its desirable ability to deal with intensity inhomogeneity in image segmentation. Furthermore, a non-negative edge detector function is used to detect the boundaries more easily. Our method has been applied to synthetic and real images with promising results. Comparisons with the split Bregman method on PC model and the original RSF model demonstrate desirable advantages of the proposed method.

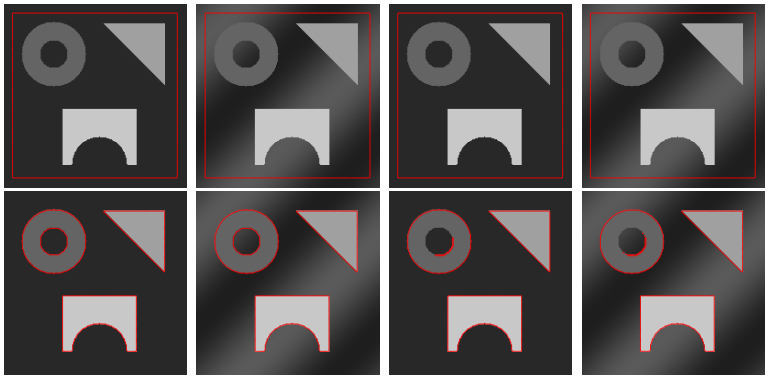

Fig. 4. Results of our method for a synthetic image. Row 1: the original image and the initial contour. Row 2: the final contour. Column 1: the piecewise constant image, $a_0 = -2$, $b_0 = 2$. Column 2: the inhomogeneous image, $a_0 = -2$, $b_0 = 2$. Column 3: the piecewise constant image, $a_0 = 0$, $b_0 = 1$. Column 4: the inhomogeneous image, $a_0 = 0$, $b_0 = 1$

Fig. 5. The result of our method for a color image of flower. It shows the curve evolution process from the initial contour to the final contour

References

1. Chan, T.F., Vese, L.A.: Active contours without edges. IEEE Trans. Image Process. **10** (2001) 266–277
2. Cohen, L., Cohen, I.: Finite element methods for active contour models and balloons for 2d and 3d images. IEEE Trans. Pattern Anal. Mach. Intell. **15** (1991) 1131–1147
3. Kass, M., Witkin, A., Terzopoulos, D.: Snakes: active contour models. Int. J. Comput. Vis. **1** (1988) 321–331
4. Malladi, R., Sethian, J.A., Vemuri, B.C.: Shape modeling with front propagation: a level set approach. IEEE Trans. Pattern Anal. Mach. Intell. **17** (1995) 158–175
5. Paragios, N., Deriche, R.: Geodesic active regions and level set methods for supervised texture segmentation. Int. J. Comput. Vis. **46** (2002) 223–247
6. Ronfard, R.: Region-based strategies for active contour models. Int. J. Comput. Vis. **13** (1994) 229–251
7. Samson, C., Blanc-Feraud, L., Aubert, G., Zerubia, J.: A variational model for image classification and restoration. IEEE Trans. Patt. Anal. Mach. Intell. **22** (2000) 460–472

8. Tsai, A., Yezzi, A., S.Willsky, A.: Curve evolution implementation of the Mumford-Shah functional for image segmentation, denoising, interpolation, and magnification. IEEE Trans. Image Process. **10** (2001) 1169–1186
9. Vese, L.A., Chan, T.F.: A multiphase level set framework for image segmentation using the Mumford and Shah model. Int. J. Comput. Vis. **50** (2002) 271–293
10. Caselles, V., Kimmel, R., Sapiro, G.: Geodesic active contours. Int. J. Comput. Vis. **22** (1997) 61–79
11. Kimmel, R., Amir, A., Bruckstein, A.: Finding shortest paths on surfaces using level set propagation. IEEE Trans. Pattern Anal. Mach. Intell. **17** (1995) 635–640
12. Li, C., Xu, C., Gui, C., Fox, M.D.: Level set evolution without re-initialization: a new variational formulation. In: Conference on Computer Vision and Pattern Recognition, IEEE (2005) 430–436
13. Vasilevskiy, A., Siddiqi, K.: Flux maximizing geometric flows. IEEE Trans. Pattern Anal. Mach. Intell. **24** (2001) 1565–1578
14. Hou, Z.: A review on MR image intensity inhomogeneity correction. Int. J. Biomed. Imag. (2006)
15. Mumford, D., Shah, J.: Optimal approximations by piecewise smooth functions and associated variational problems. Commun. Pure Appl. Math. **42** (1989) 577–685
16. Michailovich, O., Rathi, Y., Tannenbaum, A.: Image segmentation using active contours driven by the Bhattacharyya gradient flow. IEEE Trans. Image Process. **16** (2007) 2787–2801
17. Li, C., Kao, C., Gore, J.C., Ding, Z.: Minimization of region-scalable fitting energy for image segmentation. IEEE Trans. Imag. Proc. **17** (2008) 1940–1949
18. Rudin, L., Osher, S., Fatemi, E.: Nonlinear total variation based noise removal algorithms. Physica. D. (1992) 259–268
19. Goldstein, T., Osher, S.: The split Bregman method for L1 regularized problems. UCLA CAM Report 08-29 (2008)
20. Osher, S., Burger, M., Goldfarb, D., Xu, J., Yin, W.: An iterative regularization method for total variation-based image restoration. Simul. **4** (2005) 460–489
21. Houhou, N., Thiran, J.P., Bresson, X.: Fast texture segmentation based on semi-local region descriptor and active contour. Numer. Math. Theor. Meth. Appl. **2** (2009) 445–468
22. Goldstein, T., Bresson, X., Osher, S.: Geometric applications of the split Bregman method: segmentation and surface reconstruction. UCLA CAM Report 09-06 (2009)
23. Chan, T., Esedoglu, S., Nikolova, M.: Algorithms for finding global minimizers of image segmentation and denoising models. SIAM J. Appl. Math. **66** (2006) 1932–1648
24. Li, C., Kao, C., Gore, J., Ding, Z.: Implicit active contours driven by local binary fitting energy. In: Conference on Computer Vision and Pattern Recognition, Washington, DC, USA, IEEE Computer Society (2007) 1–7
25. Osher, S., Sethian, J.A.: Fronts propagating with curvature dependent speed: algorithms based on Hamilton-Jacobi formulations. J. Comput. Phys. **79** (1988) 12–49
26. Bresson, X., Esedoglu, S., Vandergheynst, P., Thiran, J., Osher, S.: Fast global minimization of the active contour/snake model. J. Math. Imag. Vis. **28** (2007) 151–167